iScience

CellPress
OPEN ACCESS

Article

Computational characterization of recombinase circuits for periodic behaviors

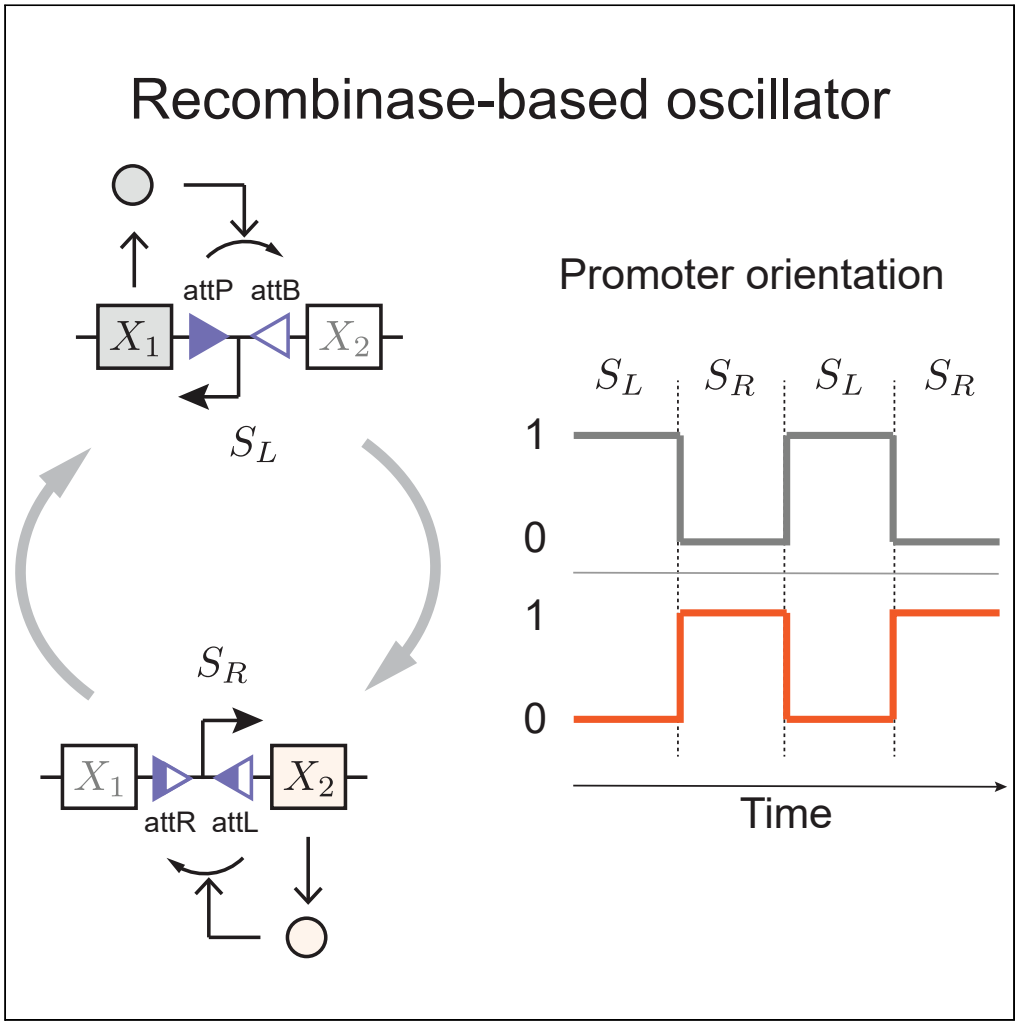

Judith Landau, Christian Cuba Samaniego, Giulia Giordano, Elisa Franco

christian.sami@gmail.com (C.C.S.)
efranco@seas.ucla.edu (E.F.)

Highlights

We design dynamical recombinase-based oscillators operating at single copy

Our designs couple two stable negative feedback loops through mutual activation

We develop a computational approach to evaluate oscillation coherence

Landau et al., iScience 26, 105624
January 20, 2023
https://doi.org/10.1016/j.isci.2022.105624

iScience

CellPress
OPEN ACCESS

Article

Computational characterization of recombinase circuits for periodic behaviors

Judith Landau,[1,4] Christian Cuba Samaniego,[2,4,*] Giulia Giordano,[3] and Elisa Franco[2,5,*]

SUMMARY

Recombinases are site-specific proteins found in nature that are capable of rearranging DNA. This function has made them promising gene editing tools in synthetic biology, as well as key elements in complex artificial gene circuits implementing Boolean logic. However, since DNA rearrangement is irreversible, it is still unclear how to use recombinases to build dynamic circuits like oscillators. In addition, this goal is challenging because a few molecules of recombinase are enough for promoter inversion, generating inherent stochasticity at low copy number. Here, we propose six different circuit designs for recombinase-based oscillators operating at a single copy number. We model them in a stochastic setting, leveraging the Gillespie algorithm for extensive simulations, and show that they can yield coherent periodic behaviors. Our results support the experimental realization of recombinase-based oscillators and, more generally, the use of recombinases to generate dynamic behaviors in synthetic biology.

INTRODUCTION

Oscillatory behaviors drive essential processes in nature. For example, the mitotic oscillator drives cell division,[1] the circadian oscillator drives the sleep-wake cycle,[2] and the segmentation clock drives spatial pattern formation during vertebrate embryonic development.[3] These numerous examples have motivated biologists, physicists, and mathematicians to look for the design principles required to build biomolecular oscillators from the bottom-up,[4,5] and many decades of theoretical and experimental research have consolidated design principles for oscillator design, which primarily include the presence of a negative feedback loop and of mechanisms for local destabilization, such as positive feedback and delays.[6–9] The implementation of these design principles within artificial genetic circuits has been shown to facilitate the emergence of periodic behaviors, in contexts spanning from single cell metabolism to multicellular environments,[10] and tremendous progress has been made toward building robust synthetic oscillators using transcription factors.[11,12] Capitalizing on these achievements, new oscillator architectures should take advantage of the rapidly expanding set of molecular parts and gene editing tools harnessed by synthetic biology.[13]

Recombinases are a class of proteins with major potential toward engineering cellular behavior.[14] These enzymes cleave and rejoin DNA strands with high specificity for given genetic domains (sequences), and many orthogonal recombinases exist. By carefully placing these domains, recombinases can perform diverse operations such as DNA excision, insertion, and translocation to generate logic and regulatory circuits that are easy to scale, and can be implemented in a variety of organisms.[15,16] Because recombinases make it possible to swap domains of DNA, they can "rewire" entire gene expression pathways. By simply inverting target promoter regions, recombinases can activate or deactivate expression with a nonlinear response that is comparable to a digital on/off switch. While this is an attractive feature toward building complex cellular circuits, the use of recombinases to generate periodic behaviors has received little attention. Creating periodic cycles of DNA site inversion using recombinases has a fundamental limitation posed by the difficulty to reverse-rearrange DNA. This limitation can be overcome by adopting serine integrases (Figure 1) which allow for reversible rearrangement of DNA, as shown in recent work toward the design of toggle switches and counters.[17,18]

In this paper, we describe and compare various candidate architectures to design oscillators using recombinases that generate regulatory feedback loops with nonlinear, switch-like responses. The simplest recombinase-based oscillator could be described as the interconnection of two negative feedback loops.

[1]California State University, Los Angeles, Los Angeles, CA, USA

[2]University of California, Los Angeles, Los Angeles, CA, USA

[3]Department of Industrial Engineering, University of Trento, Trento, Italy

[4]These authors contributed equally

[5]Lead contact

*Correspondence: christian.sami@gmail.com (C.C.S.), efranco@seas.ucla.edu (E.F.)

https://doi.org/10.1016/j.isci.2022.105624

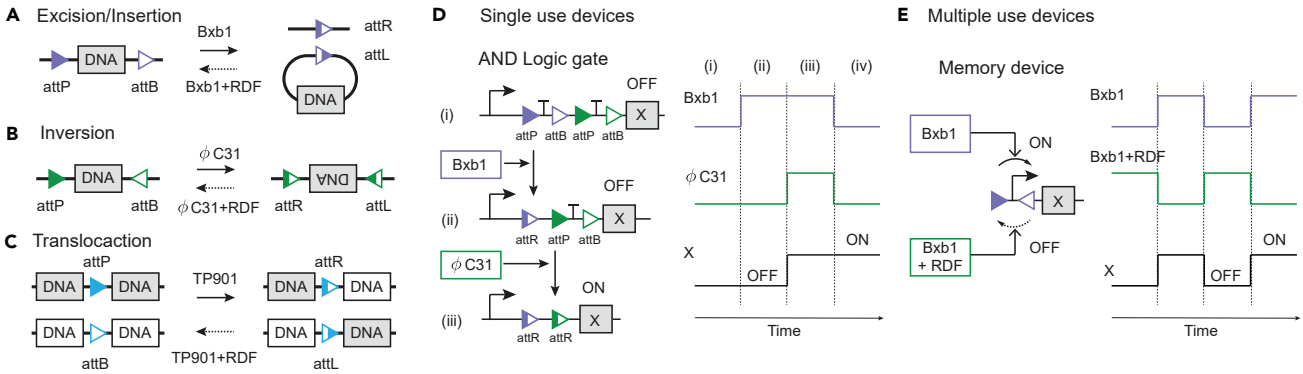

Figure 1. Serine integrases and their applications in synthetic circuits

We summarize the most important functions of serine integrases (panels A–C) and their relevant applications (panels D and E). There are two families of recombinases: tyrosine recombinases and serine recombinases.[14] All recombinases are site-specific proteins that can rearrange DNA, performing, for example, excision/insertion, inversion, and translocation. Serine integrases are a subfamily of serine recombinases, each of which has a cognate Recombination Directionality Factor (RDF) that allows the serine integrase to reverse-rearrange DNA.[14] We consider three examples involving the serine integrases Bxb1, φ C31, and TP901, with cognate attP and attB binding sites. When the attP and attB binding sites have the same orientation, Bxb1 monomers form a dimer, bind to the two specific sites, and excise the DNA segment in between, as shown in panel A (excision/insertion). When the attP and attB binding sites point in opposite directions, φ C31 binds to them and inverts the DNA between the binding sites, as shown in panel B (inversion). When the attP and attB binding sites are not in the same region of DNA, TP901 can bind to the attP and attB binding sites and translocate the DNA strands, as shown in panel C (translocation). In all the above examples, adding a recombination directional factor (RDF) enables the recombinases to recognize the binding sites attL and attR present after the rearrangements described, and therefore to reverse them. Tyrosine recombinases can perform the DNA rearrangements described, among others, but not reverse them, examples including Cre, Vre, and FLP.[19] The exception to this is the pair of tyrosine recombinases FimE and HbiF that can reverse the DNA recombination completed by the other. Recombinases have been used within logic gate circuits, such as the AND gate shown in panel D.[20] In this example, two transcription terminators are between the attP and attB binding sites for two different and orthogonal recombinases, Bxb1 and φ C31, shown in purple and green, respectively. In the absence of both recombinase inputs, the transcription of gene X is suppressed (OFF). When Bxb1 is added, it excises the first terminator. However, the transcription remains suppressed (OFF), because the second terminator is still present. When φ C31 is also added, it excises the second terminal, which finally activates the transcription of gene X (ON). Hence, two recombinase inputs (Bxb1 and φ C31) are needed to activate the circuit. One major disadvantage of recombinase-based logic gates is that the irreversibility of the DNA rearrangement means they can only be operated a single time. This circuit would require the cognate RDFs of these integrases to insert the DNA that was excised and thus be a multiple-use device. There are few demonstrations of multiple-use, dynamic devices built using recombinases. The first example was the engineering of a programmable switch, as shown in panel E.[21] This pioneering work uses Bxb1 and its RDF to change the direction of the promoter controlling the production of X over multiple cell generations.[21] An improved version of the programmable switch uses tyrosine recombinases FimE and HbiF,[22] which are the only special cases of tyrosine recombinases that allow reversible DNA rearrangement. Other dynamical circuit designs based on recombinases include a negative feedback controller to track a ref. [23,24], some theoretical designs of toggle switches that incorporate multiple copies of the circuit,[17] and a single-input counting circuit.[18] The oscillatory behavior of a recombinase-based circuit has also been analyzed deterministically.[25] Because recombinases can be used as a switch to turn on/off gene expression, they are well suited to build large Boolean logic circuits[26] that can be hierarchically composed with a predictable response.[15] In addition, self-excision recombinases were used to generate temporal responses such a pulses, and a cascade of self-excision mechanism can create a sequential pulse behavior that operates once.[16] Because leaky expression of recombinases can jeopardize circuit operation (only few protein copies are necessary to carry out their function), methods to tightly control their production are necessary, for example via light-induction.[27]

The design includes a single promoter between recombinase sites. When the promoter points to the right, the first recombinase is expressed and causes inversion of the promoter to the left. When the promoter points to the left, it drives expression of a second recombinase that causes inversion of the promoter back to the right. Thus, each recombinase suppresses its own production. Using a model based on ordinary differential equations, we previously found that this simple circuit can support periodic switching.[25] However, in any practical implementation, just a few copies of recombinase are sufficient to cause excision and inversion, so stochastic models are needed to computationally explore the circuit behavior. Moreover, it is unclear how the inherent stochasticity at low copy numbers affects the periodic switching behavior of a single-copy recombinase-based oscillator. Using the Gillespie Algorithm, we examine alternative single-copy designs incorporating different reactions to regulate more tightly the recombinase levels in the circuit, with the goal of improving the coherence of the periodic behavior. To evaluate the period incoherence, we introduce a metric based on the variance of the computationally measured autocorrelation function. We assess the effects of various reaction rate parameters on the oscillatory behavior using our period incoherence metric, and we use it as a means to compare the different designs. Overall, we find that periodic behavior is achievable in all designs when adopting biologically plausible reaction parameters. Our findings support the experimental implementation of a new class of recombinase-based oscillators.

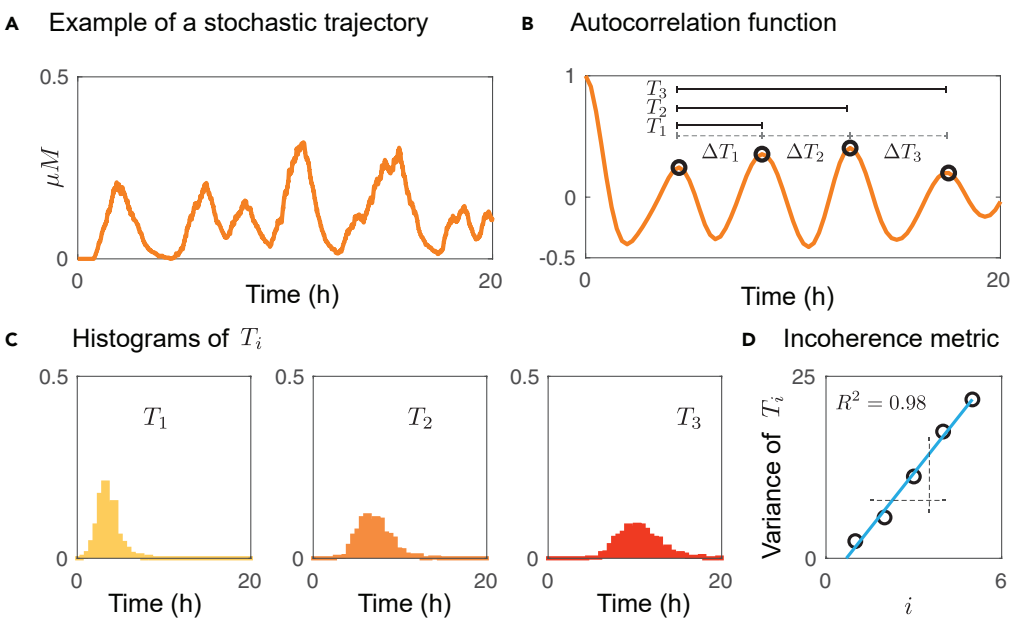

Figure 2. Incoherence metric for stochastic trajectories

(A) Example of a stochastic trajectory with periodic behavior.

(B) The autocorrelation function of the orange plot in (A) highlights the periodic cycles from the stochastic trajectory. T_i denotes the time interval between peak 1 and peak $i+1$, while the time interval between subsequent peaks $i+1$ and i is denoted as ΔT_i.

(C) Histograms showing the distributions of T_1, T_2, and T_3, when their values are taken from multiple simulations.

(D) The variance of T_i over multiple simulations plotted against i can be approximated as a line, whose slope is a metric for incoherence.

Approach

Stochastic simulations

We used the Gillespie algorithm,[28] implemented in Python, to generate stochastic trajectories of a set of species interacting according to a list of chemical reactions. The reaction rate constants (Table S1) associated with each reaction are converted to reaction propensities, and the algorithm simulates which reactions fire at each step of the simulation. The copy number increases or decreases one molecule at a time while the algorithm tracks the changes in all species over time. We study six distinct chemical reaction networks that model candidate oscillators based on recombinase interactions. Every design has a single copy of each promoter that inverts back and forth under the action of a serine integrase and the same serine integrase fused to its RDF, so the chemical reactions include promoter inversion, transcription, translation, and degradation. The left-pointing and right-pointing configurations of the promoter are considered different species: S_L and S_R, respectively. The propensity for converting from one promoter species to the other is controlled by a function of recombinase concentration since recombinase is what physically inverts the promoter. For each design, we generated 500 stochastic trajectories using a reaction volume of 1 fL; initial conditions were set to zero for all species except one copy of left-pointing promoter ($S_L = 1$).

Metrics for coherence/incoherence

To evaluate the consistency/inconsistency of the period of stochastic trajectories, we used an incoherence metric based on the autocorrelation function following the approach introduced by Yan and Paulsson.[29,30] We focus strictly on the recombinase copy number and study the coherence of the oscillation period produced by each circuit design. Fully coherent oscillations not only have a regular period but also each cycle of the oscillations has comparable amplitude. In a stochastic context, these requirements for perfect coherence are not achievable, so we only consider fluctuations of the period from the start of the simulation. Given a stochastic trajectory like the one in Figure 2A, we first compute the autocorrelation function (shown in Figure 2B) of the simulated concentration trajectory. Then, we evaluate two kinds of features of the autocorrelation function: the time interval between the first peak and each consecutive

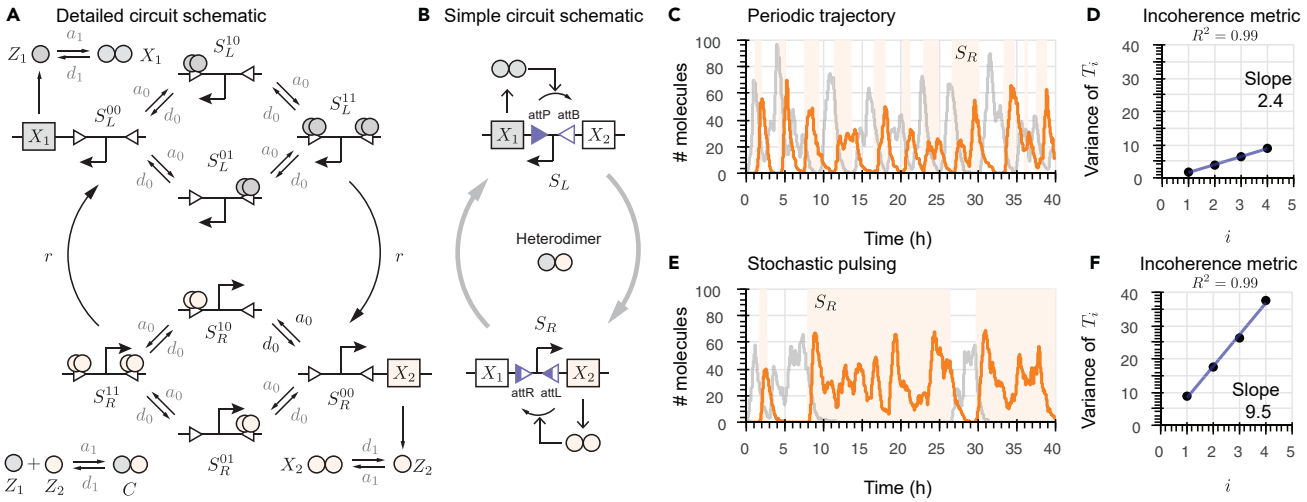

Figure 3. Architecture of a recombinase-based oscillator and incoherence of the period

(A) Detailed set of reactions of the recombinase-based oscillator design consisting of two coupled, self-inhibiting modules on the same promoter: Recombinases X_1 and X_2 can each invert the promoter when it is controlling its own production, creating a tug-of-war-like behavior. The binding sites on either side of the promoter change back and forth at each inversion.

(B) Simplified circuit representation that illustrates the two states of the promoter: left (S_L) or right (S_R).

(C) Example of a periodic trajectory achieved using the parameters in Table S1: Concentration of X_1 in gray and X_2's concentration is in orange. Light orange regions mark when the promoter points to the right (configuration S_R) and white regions mark when it points to the left (configuration S_L).

(D) Incoherence metric: Slope of the line interpolating the variance of times T_i as a function of the peak index i computed over an ensemble of 500 simulations with the simulation conditions in (C) (See also Figure 2D).

(E) Example of a trajectory exhibiting stochastic pulsing.

(F) Incoherence metric plot for the simulation conditions in (E).

peak, termed T_i, $i = 1, 2, \ldots$; and the time intervals between subsequent peaks, defined as $\Delta T_i = T_i - T_{i-1}$ for $i \geq 2$, and $\Delta T_1 = T_1$. As an example, the intervals ΔT_i and T_i are marked in Figure 2B for the first three peaks.

Given a collection of stochastic simulations, the histograms of the inter-peak time intervals ΔT_i provide direct information on the period variability; coherence in period would be associated with similar mean and variance for all the ΔT_i. It is more advantageous however to consider statistics of the T_i intervals, in particular their variance. While $T_1 = \Delta T_1$, one expects the average of T_i, $i > 1$, to increase linearly with i. While the variance of ΔT_i, $i > 1$, should not increase if oscillations are coherent, the variance of T_i does linearly increase, as fluctuations in each period are added (over each cycle) in the computation. The variance should increase proportionally to the level of "incoherence" of the oscillations. Thus, we focus on the variance of the histograms of the T_i intervals as exemplified in Figure 2C. The variance of each T_i histogram is then plotted against the peak index, as shown in Figure 2D. Because the variance of T_i is captured well by a linear fit, as shown in previous work,[30] we use the slope of the variance plot as an *incoherence metric* for the period. The variance tells us how regular the autocorrelation period is because a high variance means there is a large variety of periods. In other words, these values are irregular when variance is high. Low variance in period is required for coherent oscillations, which is the case when the metric is low. This metric was computed with our simulations of the six different designs in different parameter regimes to compare their robustness to changes in the various parameters, including recombinase translation rate constant and degradation rate constant.

RESULTS

Building a biomolecular oscillator by coupling two self-inhibiting recombinases

Our basic design for achieving periodic behavior using recombinases is shown in Figure 3A (detailed schematic) and in Figure 3B (simplified schematic). It consists of a single promoter between two recombinase binding sites, that controls the expression of two genes encoding distinct recombinase homodimers: X_1, a serine integrase that targets attP and attB binding sites, and X_2, the same serine integrase homodimer, but fused to its recombination directionality factor (RDF), which targets attR and attL binding sites (see Figure 1). The expected operation of the circuit is the following: when the promoter points to the left, with

the attP and attB binding sites on either side, it produces the recombinase X_1; when the level of X_1 is sufficiently high, it causes inversion of the promoter, pointing it to the right. In this way, X_1 inhibits its own production. When the promoter points to the right, then it has attR and attL binding sites on either side and it allows for production of recombinase X_2; in turn, X_2 causes inversion and return of the promoter to the left-pointing orientation, thereby inhibiting its own production. The coupling of these two self-inhibiting modules is expected to periodically switch the promoter between the left-pointing S_L and right-pointing S_R configurations. This has been mathematically proved in a deterministic scenario.[25] Since these are serine recombinases, the heterodimerization of the monomers Z_1 and Z_2 that forms the inactive complex C can be considered a process called molecular sequestration, which promotes the removal of the non-limiting species.[31] This process reduces the accumulation of recombinase proteins, which may be a problem for circuit operation.[25] In addition, sequestration also has the effect of introducing a delay in the system because it decreases the recombinase concentration quickly after promoter inversion and results in anti-phase behavior in the concentrations of the two recombinases. Effectively, it can be compared to a "discharge" of recombinase being produced by the circuit before promoter inversion. All of the designs in this paper incorporate sequestration. It should be noted that heterodimerization should be a faster reaction than homodimerization in order for molecular sequestration to have a noticeable improvement on oscillator performance.[11,32]

To computationally characterize the behavior of our circuits, we considered a set of chemical reactions that model transcription, translation, and sequestration interactions between recombinase monomers, and promoter inversion. The rates of these reactions were converted to reaction propensities, expressing the probability of a reaction event per unit time, and we used the Gillespie algorithm to simulate the system (see the approach section). Depending on its orientation, the promoter regulates the transcription of either mRNA M_1 (when it points to the left in configuration S_L) or mRNA M_2 (when it points to the right in configuration S_R), with rate constant θ. Thus, $S_L + S_R = 1$ for a single-copy scenario (one could adopt $S_L + S_R = N$ for a multiple-copy scenario where the number of copies is N). Both mRNAs are assumed to dilute/degrade with a rate constant φ. In addition, the mRNAs M_1 and M_2 respectively are translated to recombinase monomers Z_1 and Z_2 with rate constant ρ.

$$\begin{array}{lll} \text{Transcription:} & S_L^{00} \xrightarrow{\theta} S_L^{00} + M_1 & S_R^{00} \xrightarrow{\theta} S_R^{00} + M_2 \\ \text{mRNA Degradation:} & M_1 \xrightarrow{\varphi} \varnothing & M_2 \xrightarrow{\varphi} \varnothing \\ \text{Translation:} & M_1 \xrightarrow{\rho} M_1 + Z_1 & M_2 \xrightarrow{\rho} M_2 + Z_2 \end{array}$$

The serine recombinase monomers Z_1 and Z_2 can form the homodimers X_1 and X_2, respectively. Since Z_2 is Z_1 fused to its RDF, the two species can also form the heterodimer C. For simplicity, we assume all dimers have an association rate constant a_1 and a dissociation rate constant d_1. In addition, we assume all proteins degrade/dilute with a rate constant δ.

$$\begin{array}{ll} \text{Homodimerization:} & Z_1 + Z_1 \underset{d_1}{\overset{a_1}{\rightleftharpoons}} X_1 \qquad Z_2 + Z_2 \underset{d_1}{\overset{a_1}{\rightleftharpoons}} X_2 \\ \text{Heterodimerization:} & Z_1 + Z_2 \underset{d_1}{\overset{a_1}{\rightleftharpoons}} C. \\ \text{Protein Degradation:} & Z_1, X_1, Z_2, X_2, C \xrightarrow{\delta} \varnothing \end{array}$$

The rate of promoter inversion is regulated by the recombinase dimers X_1 and X_2 with binding and unbinding rate constants a_0 and d_0, respectively, and the inversion rate constant r.

$$\begin{array}{lll} \text{Binding/Unbinding:} & X_1 + S_L^{00} \underset{d_0}{\overset{a_0}{\rightleftharpoons}} S_L^{10} & X_1 + S_L^{10} \underset{d_0}{\overset{a_0}{\rightleftharpoons}} S_L^{11} \\ & X_1 + S_L^{00} \underset{d_0}{\overset{a_0}{\rightleftharpoons}} S_L^{01} & X_1 + S_L^{01} \underset{d_0}{\overset{a_0}{\rightleftharpoons}} S_L^{11} \\ \text{Binding/Unbinding:} & X_2 + S_R^{00} \underset{d_0}{\overset{a_0}{\rightleftharpoons}} S_R^{10} & X_2 + S_R^{10} \underset{d_0}{\overset{a_0}{\rightleftharpoons}} S_R^{11} \\ & X_2 + S_R^{00} \underset{d_0}{\overset{a_0}{\rightleftharpoons}} S_R^{01} & X_2 + S_R^{01} \underset{d_0}{\overset{a_0}{\rightleftharpoons}} S_R^{11} \\ \text{Inversion:} & S_L^{11} \xrightarrow{r} S_R^{00} + 2X_1 & S_R^{11} \xrightarrow{r} S_L^{00} + 2X_2 \end{array}$$

where the subscript L stands for a promoter oriented to the left and R for a promoter pointing to the right. The superscript S^{00} corresponds to a promoter without any recombinase dimers bound to it, S^{01} indicates a

promoter has a recombinase dimer bound to the right binding site, S^{10} represents a promoter with a recombinase dimer bound to the left binding site, and S^{11} consists of a promoter with two recombinase dimers, one bound to each binding site. In total, we have eight possible states for the promoter, four where it points to the left and four where it points to the right. Then, $S_L = S_L^{00} + S_L^{10} + S_L^{01} + S_L^{11}$, and $S_R = S_R^{00} + S_R^{10} + S_R^{01} + S_R^{11}$. With this, it still holds that $S_L + S_R = 1$ for a single copy ($S_L + S_R = N$ for N copies).

Coherence of stochastic simulations

We explored the emergence of periodic behaviors in the design described above via stochastic simulations. In particular, we wished to assess whether the circuit supports the occurrence of oscillatory solutions with a regular period. Figure 3C shows example trajectories of recombinase concentration computed using the parameters from Table S1: X_1 in gray and X_2 in orange. The light orange regions mark when the promoter points to the right (configuration S_R). The trajectories for X_1 and X_2 show oscillations with antiphase behavior, meaning that one level increases while the other decreases. Yet, since stochastic noise makes it challenging to identify a defined period, we examined coherence by computing the trajectory's autocorrelation and then calculating the inter-peak times, ΔT_i, of the autocorrelation function as shown in Figure 2B. As a metric to evaluate the incoherence of oscillations, we measured the time from the first peak of the autocorrelation function to six consecutive peaks in 500 trajectories. A small variance for these time intervals corresponds to trajectories with a small amount of change, while higher variance indicates oscillations with more change in period over time. Regardless, the variance increases approximately linearly with the peak index (See Figure 2D.). The variance of the distribution of the times, T_i, was plotted against the peak index, i (Figure 3D). We use the slope of this line as a metric to quantify the incoherence of oscillations (see STAR Methods). The lower the slope is, the more coherent the oscillations are. One can see that these lines have a very good fit since the R^2 value for each is very close to 1, as is expected for such data.[30] Also see Figure 3D.

While the circuit design in Figure 3A (or its simple representation in Figure 3B) can exhibit coherent oscillations (as shown in Figure 3C for the nominal parameters in Table S1), it can also have a switch-like behavior with significant variability of the period when parameters deviate from the nominal values. By lowering the switching rate parameter to $r/5$, for example, the system's switching behavior becomes less consistent. This means that promoter inversion becomes a random event, and we observe a regime that we call stochastic pulsing, illustrated with an example simulation in Figure 3E. Stochastic pulsing is characterized by high variance in period (as well as low variance in amplitude in some cases). Also, Figure 3F shows how fast the variance of T_i increases: the slope is 9.5 while it is 2.4 for the example of periodic trajectory, thus confirming the effectiveness of the incoherence metric. The irregular frequency of the promoter position's switching can be noted in Figure 3E by looking at the irregularly spaced, light orange bands, marking when the promoter is pointing to the right.

A range of circuit architectures can yield coherent oscillations

We next explore systematically the coherence of the oscillations when the architecture of the circuit and the values of specific parameters are varied. We focus in particular on the effects of adding different mechanisms that control the level of recombinase: repression, catalytic degradation, and activation. Because in the absence of sequestration the basic recombinase circuit did not yield coherent oscillations, we reasoned that mechanisms that introduce additional control over recombinase expression may help maintain consistent switching events in time.

We begin by considering a design that includes repressors of recombinase transcription (RR design) to push down the level of recombinase after inversion. We then consider removing recombinase molecules via proteolytic degradation (RP design). Both transcriptional repression and protease degradation, by reducing the available recombinase, have the result of delaying the next switching event.[33] We then explore three additional designs: one that regulates recombinase concentration by means of a transcriptional activator (RA design), one that incorporates the sequestration of recombinase mRNA via complementary small RNA (sRNA) species that prevent translation (RS design), and another that incorporates negative feedback.

Each of these additional reactions changes the timing of promoter switching events, and thus can change the coherence of oscillations. We used the Gillespie algorithm to generate an ensemble of trajectories for each circuit, starting with the recombinase-based oscillator we have already proposed (see Figure 3A). We

then assess the corresponding coherence of oscillations as we vary the nominal parameters in a given range.

R design: Analyzing the coherence of the recombinase-based oscillator

The R design was illustrated in Figure 3A. In Figure 4D, we examine the circuit as multiple parameters are varied, and we compare it with other circuit variants. A lower translation rate constant, ρ, results in lower recombinase concentration, which leads to stochastic pulsing as reflected in the higher values of the incoherence metric in the orange plot in Figure 4D (1). Similarly, a lower transcription rate, θ, gives rise to a higher variance in T_I. The orange plot in Figure 4D (1) also shows that a higher transcription rate reduces the incoherence metric for this circuit, thus indicating improved coherence of oscillations. However, it is worth keeping in mind that very high values of ρ can lead to very rapid switching.

Increasing the degradation rate constant, δ, can also cause stochastic pulsing by reducing the amount of recombinase in the system to very low levels, as is reflected in the high value of the incoherence metric in the orange plot in Figure 4D (2). A low degradation rate constant, δ, also corresponds to a high value of incoherence metric, also shown in the orange plot of Figure 4D (2), since it could lead to a high recombinase concentration and therefore to rapid switching. Overall, our incoherence metric indicates there is a range of δ values that yield strong coherence of oscillations, while very low or very large values hinder coherence.

The incoherence metric remains fairly constant in a wide range of a_1 values shown in the orange plot of Figure 4D (3), which means that coherence is unaffected by reasonably small changes in the value of the dimer association rate. However, decreasing a_1 by a factor of 100 does affect the incoherence metric (not shown).

On the other hand, changing a_0 values does impact the coherence of the simulations. Lower a_0 values give rise to less coherent oscillations while the oscillations produced by a circuit with higher a_0 values are much more coherent. This can be seen in the orange plot in Figure 4D (4). Since this is the binding rate constant for the recombinase-DNA complex, this means that oscillations have a more regular period when the recombinase and DNA have a greater affinity for each other.

A low switching rate, r, is associated with a high incoherence metric, and we observed this results in stochastic pulsing because the probability of inversion is lower. Conversely, increasing the value of r improves the coherence of this design (the incoherence metric is much lower), as can be seen in the orange plot in Figure 4D (4). However, higher values of r may lead to very fast switching, which may be too rapid to be classifiable as a suitable oscillation.

RR design: Transcriptional repression of recombinase production

The RR design, shown in Figure 4B (simplified schematic) along with an example trajectory, incorporates transcriptional repressors as a form of cascaded regulation. In this design, the transcription of recombinases X_1 and X_2 is regulated by transcriptional repressors Y_1 and Y_2, respectively. The production of Y_1 and Y_2 is controlled by an inverting promoter positioned between recombinase binding sites (as it was for the production of recombinases in the R design), while the genes for X_1 and X_2 have promoters regulated by Y_1 and Y_2, respectively, acting as repressors. When the promoter of the genes points to the right, Y_1 is produced, inhibiting the production of recombinase X_1. At the same time, the amount of recombinase X_2 increases because Y_2 is not being produced. This causes the promoter to invert to the left. As a consequence, the production of Y_2 increases while Y_1 decreases in concentration due to decay. The remaining Y_1 still blocks the production of X_1 until its level is too low for repression. When Y_2 is high in concentration and Y_1 is low, the amount of recombinase X_1 increases and eventually becomes sufficient to invert the promoter to the right. In addition, Y_2 delays the production of X_2 until the concentration of Y_2 becomes low enough, making it unable to repress the production of X_2. This sequence of steps is expected to repeat as the promoters invert back and forth. Overall, the repressors introduce a lag in the response time of the system because each repressor protein remains present after promoter inversion and continues to repress its associated promoter effectively. Additional time is required for the repressor to decay to levels where it no longer represses the production of its associated recombinase. The sequestration reaction between recombinases further helps keep the less abundant recombinase species inactive, thereby preventing stochastic pulsing and promoting more coherent oscillations.

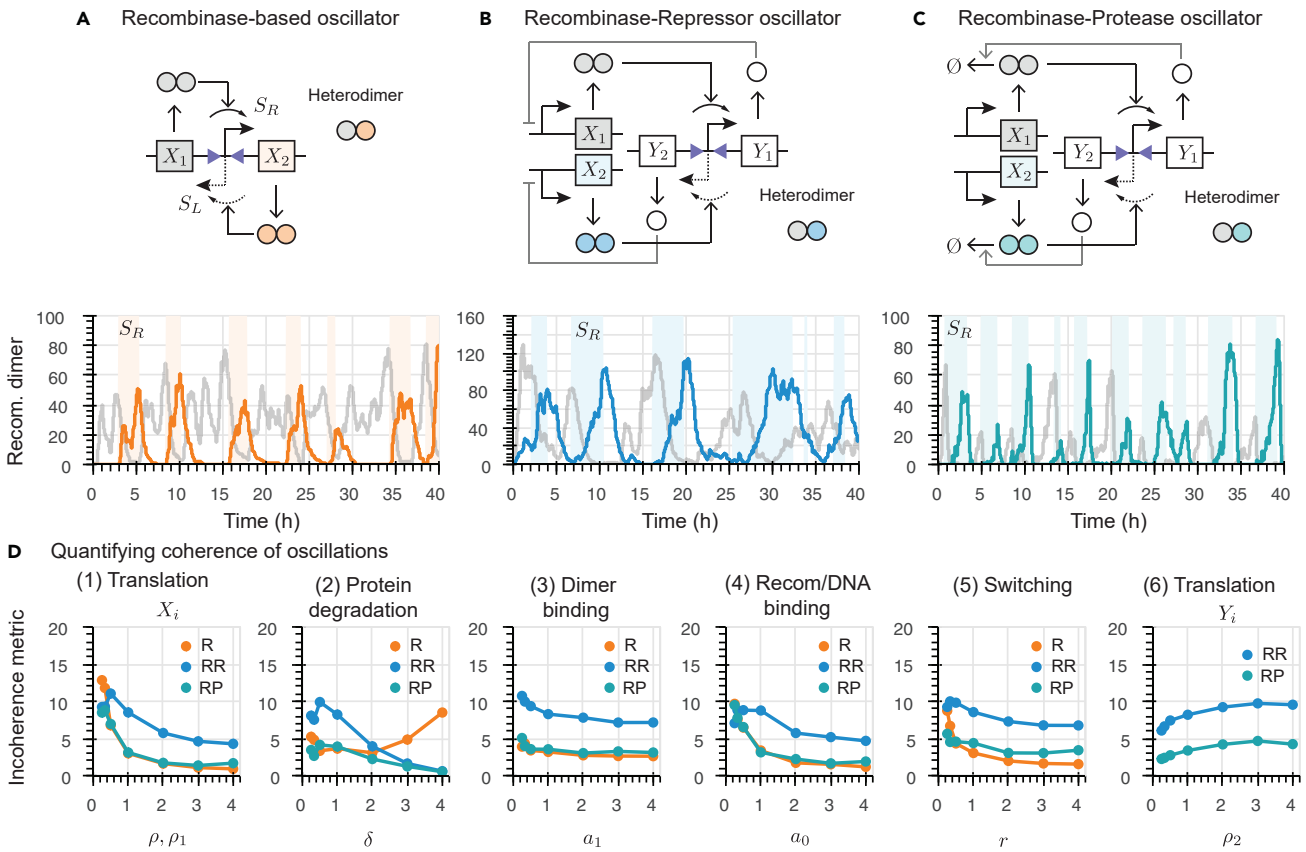

Figure 4. Analysis of the R, RR, and RP oscillator designs

(A) Top: R oscillator design with a single inverting promoter that alternately controls the production of recombinases X_1 (when it is pointing to the left, configuration S_L) and X_2 (when it is pointing to the right, configuration S_R). Molecular sequestration is included through the heterodimerization of X_1 and X_2. Bottom: Trajectories of a single simulation showing the time evolution of the concentrations of X_1 (gray) and X_2 (orange) over time. The light orange stripes mark when the promoter points to the right (configuration S_R), while white stripes mark when the promoter points to the left (configuration S_L).

(B) Top: RR oscillator design with a single inverting promoter that alternately controls the production of two different repressor proteins, Y_1 and Y_2, while recombinases X_1 and X_2 are produced constitutively and also heterodimerize. Bottom: Trajectories of a single simulation showing the time evolution of the concentrations X_1 (gray) and X_2 (blue). The colored stripes indicate the current promoter configuration (S_R or S_L).

(C) Top: RP oscillator design with an inverting promoter that alternates between controlling the production of protease proteins Y_1 and Y_2, while recombinases X_1 and X_2 are produced constitutively with the ability to heterodimerize. Bottom: Trajectories of a single simulation showing the time evolution of X_1 (gray) and X_2 (teal). The colored stripes denote the current promoter configuration (S_R or S_L).

(D) Analysis of the coherence of the R, RR, and RP designs for different parameter regimes. Each point on these plots represents the incoherence metric calculated using a collection of simulations using the multiplier value indicated on the x axis. All parameters used for our simulations are reported in Table S1 along with their nominal values. For our sensitivity analysis, in each plot, we vary the considered parameter value from 0.25 to 4 times its nominal value.

We developed a model for the RR circuit (Figure 4B), reported here as a list of chemical reactions, including transcription and translation. Rate constants were converted to propensities to simulate the reactions using the Gillespie algorithm. We then studied the periodic behavior of this circuit under different parameter values.

The inverting promoter regulates the transcription of either of the two mRNA repressors, W_1 and W_2, with rate constant β at any given time. W_1 is produced when the promoter is pointing to the right (configuration S_R) and W_2 is produced when the promoter is pointing to the left (configuration S_L). The mRNAs also decay with a rate constant φ.

$$\text{Transcription:} \quad S_R^{00} \xrightarrow{\beta} S_R^{00} + W_1 \qquad S_L^{00} \xrightarrow{\beta} S_L^{00} + W_2$$

$$\text{mRNA Degradation:} \quad W_1 \xrightarrow{\varphi} \varnothing \qquad W_2 \xrightarrow{\varphi} \varnothing.$$

W_1 and W_2 are translated into repressors proteins Y_1 and Y_2 with a rate constant ρ_2 and decay with a rate constant δ.

$$\begin{array}{ll} \text{Translation:} & W_1 \xrightarrow{\rho_2} W_1 + Y_1 \qquad W_2 \xrightarrow{\rho_2} W_2 + Y_2 \\ \text{Protein Degradation:} & Y_1 \xrightarrow{\delta} \varnothing \qquad Y_2 \xrightarrow{\delta} \varnothing. \end{array}$$

The repressors Y_1 and Y_2 bind and unbind to target promoters P_1 and P_2, making them promoters P_1^* and P_2^*, at rates a_R and d_R, respectively. The unbound promoters, P_1 and P_2, regulate the transcription rate of recombinase mRNAs M_1 and M_2 with parameter θ. Both mRNAs decay with a rate constant φ. In addition, the mRNAs produce recombinase monomers Z_1 and Z_2 with a rate constant ρ_1.

$$\begin{array}{ll} \text{Binding/Unbinding:} & Y_1 + P_1 \underset{d_R}{\overset{a_R}{\rightleftharpoons}} P_1^* \qquad Y_2 + P_2 \underset{d_R}{\overset{a_R}{\rightleftharpoons}} P_2^* \\ \text{Transcription:} & P_1 \xrightarrow{\theta} P_1 + M_1 \qquad P_2 \xrightarrow{\theta} P_2 + M_2 \\ \text{mRNA Degradation:} & M_1 \xrightarrow{\varphi} \varnothing \qquad M_2 \xrightarrow{\varphi} \varnothing \\ \text{Translation:} & M_1 \xrightarrow{\rho_1} M_1 + Z_1 \qquad M_2 \xrightarrow{\rho_1} M_2 + Z_2. \end{array}$$

The monomers Z_1 and Z_2 form homodimers X_1 and X_2 in addition to heterodimer C, both with an association rate constant a_1 and a dissociation rate constant d_1. The heterodimer formation is possible because the second recombinase monomer is fused to its RDF. In addition, all protein complexes decay with a rate constant δ.

$$\begin{array}{ll} \text{Homodimerization:} & Z_1 + Z_1 \underset{d_1}{\overset{a_1}{\rightleftharpoons}} X_1 \qquad Z_2 + Z_2 \underset{d_1}{\overset{a_1}{\rightleftharpoons}} X_2 \\ \text{Heterodimerization:} & Z_1 + Z_2 \underset{d_1}{\overset{a_1}{\rightleftharpoons}} C. \\ \text{Protein Degradation:} & Z_1, X_1, Z_2, X_2, C \xrightarrow{\delta} \varnothing \end{array}$$

Finally, the switching rate of the promoter is regulated by the recombinase dimers X_1 and X_2 with binding rate constant a_0 and unbinding rate constant d_0.

$$\begin{array}{ll} \text{Binding/Unbinding:} & X_1 + S_L^{00} \underset{d_0}{\overset{a_0}{\rightleftharpoons}} S_L^{10} \qquad X_1 + S_L^{10} \underset{d_0}{\overset{a_0}{\rightleftharpoons}} S_L^{11} \\ & X_1 + S_L^{00} \underset{d_0}{\overset{a_0}{\rightleftharpoons}} S_L^{01} \qquad X_1 + S_L^{01} \underset{d_0}{\overset{a_0}{\rightleftharpoons}} S_L^{11} \\ \text{Binding/Unbinding:} & X_2 + S_R^{00} \underset{d_0}{\overset{a_0}{\rightleftharpoons}} S_R^{10} \qquad X_2 + S_R^{10} \underset{d_0}{\overset{a_0}{\rightleftharpoons}} S_R^{11} \\ & X_2 + S_R^{00} \underset{d_0}{\overset{a_0}{\rightleftharpoons}} S_R^{01} \qquad X_2 + S_R^{01} \underset{d_0}{\overset{a_0}{\rightleftharpoons}} S_R^{11} \\ \text{Inversion:} & S_L^{11} \xrightarrow{r} S_R^{00} + 2X_1 \qquad S_R^{11} \xrightarrow{r} S_L^{00} + 2X_2 \end{array}$$

As shown in the blue plot in Figure 4D (1), the RR design has a high incoherence metric for low values of translation rate constant, ρ_1, while coherence increases for higher ρ_1 values, but not to the same extent as it does for the R design. Similarly, high ρ_1 can lead to fast switching and low ρ_1 can give rise to stochastic pulsing. The blue plot in Figure 4D (2) shows that the RR oscillator is quite coherent for high values of protein degradation δ, but rather incoherent for low values of δ. This is because the coherent simulations for this oscillator have a large period, so a longer simulation is required to properly ascertain an accurate coherence metric. However, this was not provided to keep the comparisons in this paper consistent.

Coherence is unaffected by a_1 in the RR design, but is lower in general, as shown in the blue plot in Figure 4D (3) unless a_1 is decreased by a factor of 100 (not shown). The blue plot in Figure 4D (4) shows that, as for the R design, the incoherence metric becomes higher as the a_0 value of the RR design decreases, revealing poor coherence between periods because promoter inversion is induced poorly by the lack of a recombinase/DNA complex, S_L^{11} or S_R^{11}. This design also has a high incoherence metric for low values of the switching rate, r, while the incoherence metric gets lower when r is high, as shown in the blue plot in Figure 4D (5). There is also a small increase in the incoherence metric as the repressor translation rate, ρ_2, increases, as shown in the blue plot in Figure 4D (6).

RP design: Introducing protease-based regulation

Since slowly decaying recombinases lead to higher rates of inversion for the R design (Figure 4D (2), orange plot), we reasoned that regulating the decay rate could improve the switching behavior of an oscillator. Next, we analyze a circuit design that relies on proteases to control the amount of active recombinase present. Others have created similar circuit designs using protease in the past.[34] The simple circuit schematic is

shown in Figure 4C, along with an example trajectory. Proteases are proteins that can cleave a polypeptide at a specific, targeted amino acid sequence so as to inhibit its function.[35,36] The RP circuit design consists of recombinases X_1 and X_2 that are cleaved by two orthogonal proteases Y_1 and Y_2, respectively. When the inverting promoter points to the right, it produces the protease Y_1, which selectively cleaves the recombinase X_1. At the same time, the amount of recombinase X_2 increases due to the lack of protease Y_2. Then X_2 inverts the promoter to the left, initiating the production of protease Y_2 and leaving Y_1 to decrease in concentration due to degradation. However, the remaining Y_1 continues to target and cleave X_1. This delays the increase in the amount of X_1. After this delay, X_1 eventually inverts the promoter to the right and stops the production of Y_2. The remaining amount of Y_2 will delay the production of recombinase X_2 before it can then effectively invert the promoter to the left. These interactions are expected to generate a repetitive switching behavior in which the promoter is inverted from right to left back and forth, but the half-cycle of each oscillation is expected to be longer when compared to the R design.

As in the previous cases, we built a model to evaluate the dynamics of the RP circuit design shown in Figure 4C. Constitutive transcription of recombinase mRNAs M_1 and M_2 occurs at a constant rate, θ, and decay at a constant rate, φ. In addition, the mRNAs produce recombinase monomers Z_1 and Z_2 with a rate constant ρ_1.

$$\begin{array}{rcc} \text{Transcription:} & \varnothing \xrightarrow{\theta} M_1 & \varnothing \xrightarrow{\theta} M_2 \\ \text{mRNA Degradation:} & M_1 \xrightarrow{\varphi} \varnothing & M_2 \xrightarrow{\varphi} \varnothing \\ \text{Translation:} & M_1 \xrightarrow{\rho_1} M_1 + Z_1 & M_2 \xrightarrow{\rho_1} M_2 + Z_2. \end{array}$$

The monomers Z_1 and Z_2 can form homodimers X_1 and X_2, respectively, as well as heterodimer C with association rate constant a_1 and dissociation rate constant d_1. The heterodimer formation is possible because the second recombinase monomer is fused to its RDF. In addition, all protein complexes decay with a rate constant δ.

$$\begin{array}{rcc} \text{Homodimerization:} & Z_1 + Z_1 \underset{d_1}{\overset{a_1}{\rightleftharpoons}} X_1 & Z_2 + Z_2 \underset{d_1}{\overset{a_1}{\rightleftharpoons}} X_2 \\ \text{Heterodimerization:} & Z_1 + Z_2 \underset{d_1}{\overset{a_1}{\rightleftharpoons}} C. & \\ \text{Protein Degradation:} & Z_1, X_1, Z_2, X_2, C \xrightarrow{\delta} \varnothing & \end{array}$$

The inverting promoter, located between recombinase binding sites, regulates the transcription of protease mRNAs W_1 and W_2 with rate parameter β. Protease mRNAs are also degraded/diluted with rate parameter φ.

$$\begin{array}{rcc} \text{Transcription:} & S_R \xrightarrow{\beta} S_R + W_1 & S_L \xrightarrow{\beta} S_L + W_2 \\ \text{mRNA Degradation:} & W_1 \xrightarrow{\varphi} \varnothing & W_2 \xrightarrow{\varphi} \varnothing. \end{array}$$

The mRNA species W_1 and W_2 yield proteases Y_1 and Y_2, each with a rate constant ρ_2. The protease proteins decay with a rate constant δ.

$$\begin{array}{rcc} \text{Translation:} & W_1 \xrightarrow{\rho_2} W_1 + Y_1 & W_2 \xrightarrow{\rho_2} W_2 + Y_2 \\ \text{Protein Degradation:} & Y_1 \xrightarrow{\delta} \varnothing & Y_2 \xrightarrow{\delta} \varnothing. \end{array}$$

The protease Y_1 (respectively Y_2) targets the recombinase monomer Z_1 (respectively Z_2) as well as dimer X_1 (respectively X_2) for catalytic degradation. Since we have both a high protease and recombinase copy number, we decided to model the cleavage of recombinase by protease using Hill function-type propensities, consistently with previous literature;[37] this choice also has the advantage of reducing the model complexity. Protease reactions occur with rate parameters g_1 and g_2, corresponding to a Hill-type function with Hill coeffiecient equal to 1.

$$\begin{array}{rcc} \text{Catalytic Protein Degradation:} & Y_1 + Z_1 \xrightarrow{g_1} Y_1 & Y_1 + X_1 \xrightarrow{g_1} Y_1 \\ \text{Catalytic Protein Degradation:} & Y_2 + Z_2 \xrightarrow{g_2} Y_2 & Y_2 + X_2 \xrightarrow{g_2} Y_2, \end{array}$$

where $g_1 = \xi \frac{1}{z_1 + x_1 + K_d}$ and $g_2 = \xi \frac{1}{z_2 + x_2 + K_d}$.

Finally, the switching rate constant of the promoter is regulated by the recombinase dimers X_1 and X_2 with binding rate constant a_0 and unbinding rate constant d_0 as shown.

$$\text{Binding/Unbinding:}\quad X_1 + S_L^{00} \underset{d_0}{\overset{a_0}{\rightleftharpoons}} S_L^{10} \qquad X_1 + S_L^{10} \underset{d_0}{\overset{a_0}{\rightleftharpoons}} S_L^{11}$$

$$X_1 + S_L^{00} \underset{d_0}{\overset{a_0}{\rightleftharpoons}} S_L^{01} \qquad X_1 + S_L^{01} \underset{d_0}{\overset{a_0}{\rightleftharpoons}} S_L^{11}$$

$$\text{Binding/Unbinding:}\quad X_2 + S_R^{00} \underset{d_0}{\overset{a_0}{\rightleftharpoons}} S_R^{10} \qquad X_2 + S_R^{10} \underset{d_0}{\overset{a_0}{\rightleftharpoons}} S_R^{11}$$

$$X_2 + S_R^{00} \underset{d_0}{\overset{a_0}{\rightleftharpoons}} S_R^{01} \qquad X_2 + S_R^{01} \underset{d_0}{\overset{a_0}{\rightleftharpoons}} S_R^{11}$$

$$\text{Inversion:}\quad S_L^{11} \xrightarrow{r} S_R^{00} + 2X_1 \qquad S_R^{11} \xrightarrow{r} S_L^{00} + 2X_2$$

Like the previous designs, the incoherence metric of the RP design is high at low ρ_1 values, and it decreases as ρ_1 increases, as shown in the teal plot in Figure 4D (1). Hence, a large ρ_1 improves the coherence of oscillations. In contrast with other designs, this case has a remarkably low incoherence metric for low degradation rate constant, δ, as show in the teal plot in Figure 4D (2). This indicates that stochastic pulsing does not occur at low degradation rates. For this reason, this design is the most robust to changes in δ, among all the designs we have considered so far. Again, varying a_1 does not affect coherence (Figure 4D (3), teal plot), unless a_1 is decreased by a factor of 100. As in the R design, the teal plot in Figure 4D (4) shows that coherence increases as a_0 increases in the RP design. As we have described in the R and RR oscillators, for the RP design, a low r value is associated with a higher incoherence metric, which decreases as r increases. However, the metric increases as r becomes large in the RP design. This is shown in the teal plot in Figure 4D (5).

The teal plot in Figure 4D (6) shows the effect of increasing the protease translation rate, ρ_2: the incoherence metric increases slightly as ρ_2 increases, following the same trend observed when varying ρ_2 in the RR oscillator (repressor protein translation rate).

Additional architectures

Here, we briefly describe three additional architectures where recombinase levels are regulated with different approaches. The derivation of the model for each circuit design can be found in the STAR Methods.

An activator-based circuit design (RA design)

The RA circuit design incorporates an activator to regulate recombinase production. The corresponding schematic is reported in Figure 5A along with an example trajectory. The design consists of the transcriptional activators Y_1 and Y_2 that drive the production of recombinases X_1 and X_2. When the inverting promoter points to the left, it produces the activator Y_1, driving the production of X_1. These two steps in the cascade must occur before X_1 can be produced and hence slow down the production of the recombinase. Once X_1 increases in concentration, it can invert the promoter to the right. This leads to the production of Y_2 and stops the production of Y_1. Then, Y_2 increases the production of X_2. When X_2 increases in concentration, it can invert the promoter to the left. Overall, this leads to a switching cycle of inverting the promoter from left to right repeatedly. One challenge with this design is that, even when an activator is not being produced, the remaining transcription factor can still increase the production of its associated recombinase. This makes it difficult for the concentration of each recombinase to get very low, which causes the promoter to invert more irregularly.

As a result, the RA design is the worst-performing among the designs we tested. The incoherence metric is consistently higher than that of the other oscillators in nearly every parameter regime. When ρ_1 is varied, the incoherence metric follows the same pattern as that of previous designs, decreasing as ρ_1 increases (Figure 5D (1), blue plot). The window of δ values for which this oscillator is more coherent (Figure 5D (2), blue plot) is also the smallest.

Parameter a_1 also does not affect coherence in this design, as shown by the blue plot in Figure 5D (3), unless it is decreased by a factor of 100. However, the incoherence metric is higher overall for the RA oscillator compared to the other designs. The blue plot in Figure 5D (4) follows the general pattern of this plot for the other designs, the incoherence metric decreasing as a_0 increases. While the incoherence metric does decrease as r increases, it again remains higher than for the other oscillators over the entire range of r values we tested with the exception of the RR oscillator, which is fairly comparable to the RA oscillator in this regard (Figure 5D (5), blue plot).

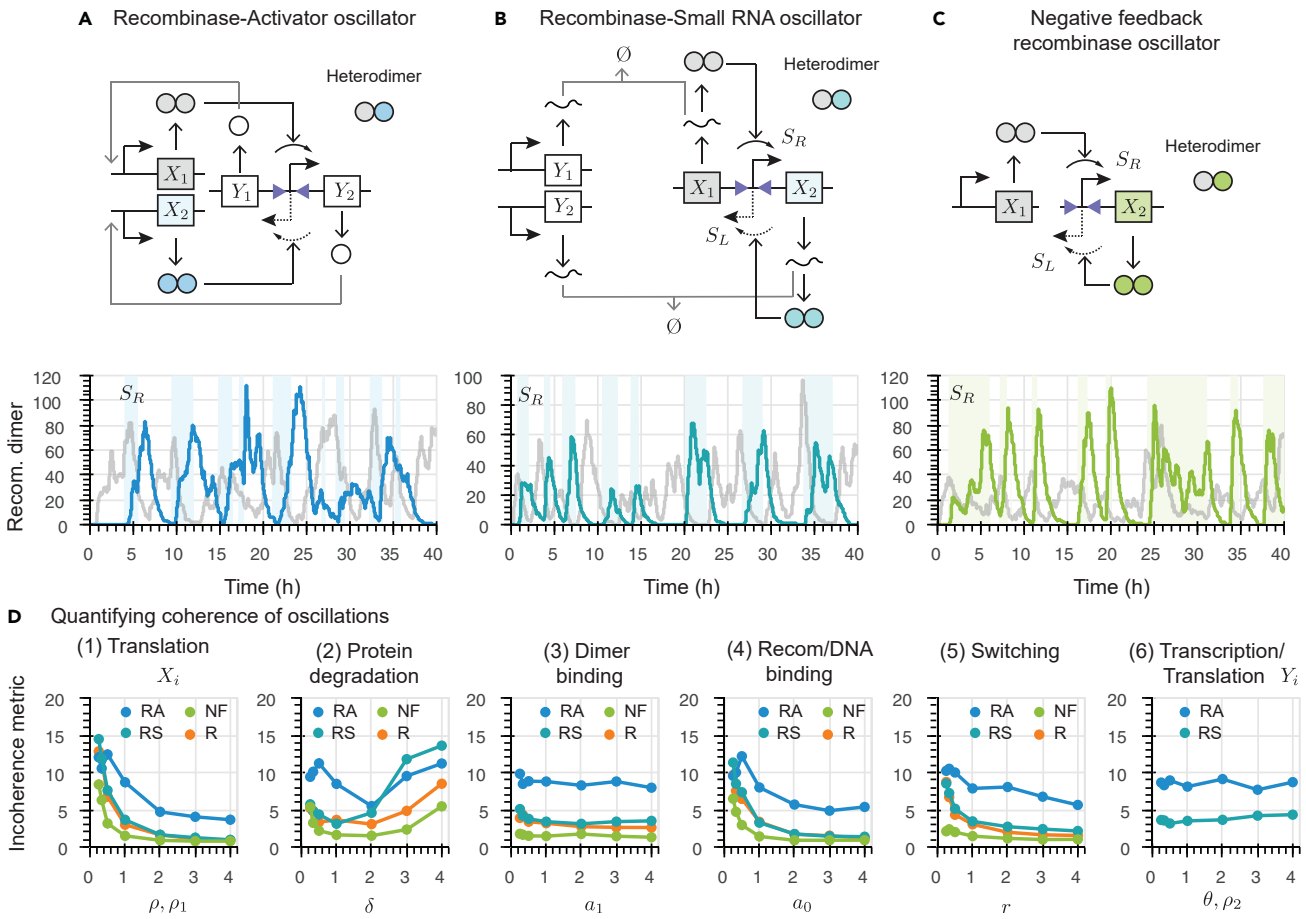

Figure 5. Analysis of the RA, RS, and NF oscillator designs

(A) Top: RA oscillator design with a single inverting promoter that alternately controls the production of transcriptional activators Y_1 and Y_2, which respectively regulate the production of recomabinases dimers X_1 and X_2; the recombinase monomers undergo molecular sequestration through heterodimerization. Bottom: Trajectories of a single illustrative simulation showing the time evolution of the concentrations of X_1 (gray) and X_2 (blue) over time. The light color stripes mark when the promoter points to the right (configuration S_R), while white stripes mark when the promoter points to the left (configuration S_L).

(B) Top: RS oscillator design with an inverting promoter that alternately regulates the production of small RNAs Y_1 and Y_2, which inhibit mRNA recombinases, preventing their transcription into X_1 and X_2, respectively. These recombinases are also able to heterodimerize. Bottom: Trajectories of a single simulation showing the time evolution of the concentrations of X_1 (gray) and X_2 (teal). The colored stripes indicate the current promoter configuration (S_R or S_L).

(C) Top: NF oscillator design with a single self-inhibiting module controlling the production of X_2 and a constitutive promoter controlling the production of X_1, with recombinase monomers sequestering into heterodimers. Bottom: Trajectories of a single simulation showing the time evolution of X_1 (gray) and X_2 (green). The colored stripes denote the current promoter configuration (S_R or S_L).

(D) Analysis of the coherence of the RA, RS, and NF designs for different parameter regimes. Each point on these plots represents the incoherence metric calculated using a collection of simulations, using the parameter value indicated on the x axis. All other parameters used for our simulations are reported in Table S1 along with their nominal values. For our sensitivity analysis, in each plot we vary the considered parameter value from 0.25 to 4 times its nominal value.

Finally, the activator translation rate, ρ_2, does not affect the coherence of the oscillator very much (Figure 5D (6), blue plot), a pattern noticeably different from that shown by the other oscillators with an additional element in their cascade that we have discussed so far. We will see it is more similar to this pattern for the next oscillator we consider.

An sRNA-based circuit design (RS design)

Molecular sequestration can program temporal delays by setting concentration thresholds.[38] The time that the system takes to reach this threshold defines the delay caused by sequestration. We take inspiration from this mechanism to design a circuit that sequesters recombinase mRNA with small RNA as shown in Figure 5B, which reports the schematic as well as an example trajectory. The circuit consists of small

RNA molecules Y_1 and Y_2 that target the recombinase mRNAs X_1 and X_2, respectively. When the inverting promoter points to the right, it produces the recombinase mRNA X_2, which is sequestered by the small RNA Y_2. Since only X_2 is being produced without X_1, the concentration of the recombinase transcribed from X_2 increasing to overcome this sequestration results in the inversion of the promoter to the left. Then, the amount of recombinase mRNA X_1 increases while X_2 decays. Once X_1 increases in concentration to overcome its sequestration by Y_1, the recombinase transcribed from X_1 inverts the promoter to the right. This results in the continuous inversion of the promoter from left to right where the delay is caused by the time it takes for recombinase mRNA concentration to reach the threshold where it overcomes its sequestration by sRNA.

The incoherence metric for varying ρ_1 values (Figure 5D (1), teal plot) is akin to that for the R, RR, and RP designs. Compared to the RA oscillator, the RS oscillator has a broader range of δ values for which the incoherence metric is low (Figure 5D (2), teal plot). Like in all other designs, a_1 does not affect coherence (Figure 5D (3), teal plot) unless it is decreased by a factor of 100. The incoherence metric follows the same overall pattern with the regard to a_0 as all of the oscillators, decreasing as a_0 increases (Figure 5D (4), teal plot). For the RS oscillator, the incoherence metric also decreases as r increases, which is similarly in line with the general behavior for the R, RR, and RP designs (Figure 5D (5), teal plot).

Interestingly, the incoherence metric increases slightly as θ, the translation rate of the sRNA, increases (Figure 5D (6), teal plot). This follows the same pattern as all of the other oscillators with an additional regulatory component with regard to ρ_2, which controls the production rate of such factor.

Negative feedback oscillator (NF design)

The NF design, whose schematic is shown in Figure 5C along with an example trajectory, consists of a constitutive promoter controlling the production of recombinase X_1 and a self-inhibitory module regulating recombinase X_2. The presence of two distinct promoters differentiates this design from the circuit design in Figure 4A, which contains a single promoter. The regulation (or orientation) of the promoter controlling the production of X_2 experiences the effect of suppression by negative feedback, strengthened by heretodimer formation by recombinase monomers. This circuit can exhibit switching behavior with a consistent period, as well as stochastic pulsing behavior. When the total production rate of X_2 is larger than that of X_1, X_2 not only inhibits its own production by causing its promoter to point to the left but also limits the homodimer formation of X_1. When Z_2 monomers are no longer being produced, they become depleted by sequestration. Only then does the concentration of X_1 have the opportunity to increase, which inverts the promoter to the right (configuration S_R). This results in periodic behavior with a consistent period. Conversely, stochastic pulsing occurs when the level of X_1 is very low and the inversion of the promoter to the right occurs randomly. On the other hand, when the concentration of X_1 is larger than that of X_2, the system yields very fast oscillations, because X_1 is readily available to flip the promoter to the state S_R. This fast promoter inversion may be the reason behind the circuit's low incoherence metric when compared to all the other variants, as shown in Figure 5D. The effect of the various parameters is akin to that observed for the other circuits.

Interpreting the coherence of oscillations through the analysis of single self-inhibiting circuits

To interpret and explain the emergence of incoherent oscillations in our basic architecture (Figure 3B), which consists of two interconnected self-inhibitory modules, we examined the behavior of a single self-inhibitor. We reasoned that a single module contributes to half of each oscillatory cycle and its analysis could provide qualitative insights into the behavior of the full system. We computed the time it takes for inversion to occur, denoted T_I, and the recombinase concentration at inversion, denoted X_I. Both quantities have statistical properties that make it possible to determine the impact of noise propagation on the switching behavior. Furthermore, the analysis of T_I and X_I contributes to the identification of key network parameters that mitigate the phase change in the oscillations.

A schematic of the self-inhibiting module is in Figure 6A; the set of chemical reactions we modeled is in the STAR Methods.

All stochastic simulations of the self-inhibiting module produce a pulse in recombinase concentration, as shown by the gray trajectories in Figure 6B (top). This pulse can be viewed as half of an oscillatory cycle, and occurs when the promoter is in the on-state (S_R), until the level of recombinase is sufficiently high to elicit

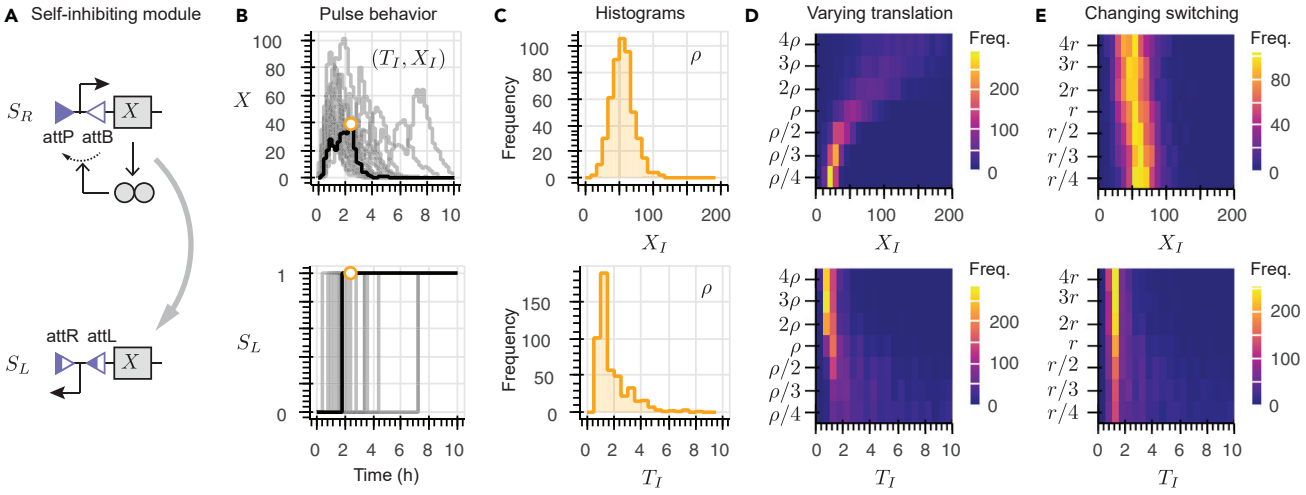

Figure 6. Analysis of the self-inhibiting module

(A) Schematic describing the operation of the self-inhibiting module. Top: The promoter points to the right (configuration S_R) and thus allows for the production of recombinase X, which inverts the promoter. Bottom: After inversion, the promoter points to the left (configuration S_L) and the recombinase X is no longer produced.

(B) Top: 10 example stochastic trajectories of the self-inhibiting module. All the trajectories show a pulse-like behavior because the number of molecules of X increases until the promoter is inverted and the production of X stops at which point the level of X decays due to dilution/degradation. Bottom: Promoter position over time for each simulation. For all the simulations, the promoter initially points to the right (configuration S_R) and eventually points to the left (configuration S_L). The inversion time is denoted as T_I and the recombinase copy number at inversion is X_I.

(C) For 500 simulations with a recombinase translation rate constant, ρ, the histograms show the relative frequency of two important quantities. Top: Histogram of recombinase copy number at inversion, X_I; this variable has a low variance. Bottom: Histogram of the inversion time, T_I; here we observe a high variance.

(D) Top: Heatmap where each row represents a histogram of the recombinase copy number at inversion, X_I, for 500 simulations with a different translation rate constant, ρ. Bottom: Heatmap where each row represents a histogram of the inversion time, T_I, for 500 simulations with different translation rate constant, ρ.

(E) Top: Heatmap where each row represents a histogram of the recombinase copy number at inversion, X_I, for 500 simulations in which the switching rate r is varied. Bottom: Heatmap where each row represents a histogram of the inversion time, T_I, for 500 simulations, each with a different r value.

inversion of the promoter to the off-state (S_L). When the promoter is off, the recombinase level decreases due to dilution/degradation. Each trajectory presents a distinct promoter inversion time, T_I, and recombinase concentration at the point of inversion, X_I. We mark these quantities in Figure 6B for the trajectory in black. The top and bottom panels of Figure 6C respectively show the histograms of the relative frequency of X_I values and of T_I values for 500 simulations, using the nominal parameters in Table S1. While X_I has small variance, T_I has a large variance, indicating that the half-cycle of an oscillator using this particular transcription rate would have an irregular period. Thus, many consecutive, irregular half-cycles could cause the oscillator to become out of phase very quickly.

We sought to gain a more comprehensive understanding of how the histograms of X_I and T_I are affected by the circuit parameters. Figures 6D and 6E show heat maps representing the computed distribution of X_I (top) and T_I (bottom). Each row of these plots should be interpreted as a color-coded histogram of X_i and T_i corresponding to a different translation rate constant, ρ (Figure 6D), and switching rate parameter, r (Figure 6E). Higher translation rates reduce both the mean and the variance of T_I, but introduce a high variance for X_I. When two such self-inhibiting modules are interconnected to build an oscillator (Figure 3A), we see that a high recombinase translation rate yields a low incoherence metric in all architectures (Figures 4D (1) and 5D (1)), which indicates that a consistent switching time may be crucial for coherence. It is important to remember that a low incoherence metric may be associated with rapid switching, as suggested by the low mean of T_I. In contrast, small values of ρ lead to a reduced variance for X_I, but to an increased variance for T_I (Figure 6D). This larger variance of the inversion time may be the reason why in the complete oscillator (Figure 3A) a low recombinase translation rate constant causes stochastic pulsing and high incoherence.

In Figure 6E, we varied the switching rate parameter, r, which scales the inversion of the promoter. Overall, a lower value for r leads to higher variance in the distribution of T_I, and hence the trajectories of the

corresponding full oscillator design in Figure 3A exhibit stochastic pulsing for low r values. In contrast, a high r value results in small mean and variance for both T_I and X_I, which may improve the coherence of oscillations: this is consistent with the simulations of the full circuit variants in Figures 4D (5) and 5D (5). Overall, while not predictive, these simulations indicate that examining an individual self-inhibiting module is useful to interpret the behavior of the full circuit.

Limitations of the study

Coherent oscillations should have comparable period, phase, and amplitude throughout their duration. Our approach focuses exclusively on period consistency, and broad progress in this context will require the development of methods for examining phase and amplitude consistency as well. It is important to note that our notion of coherence does not provide information on the period duration. First, we note that small stochastic fluctuations in the recombinase trajectories are always captured when computing the autocorrelation function, and thus contribute to the incoherence metric; these fluctuations are due to the presence of multiple reaction steps like promoter inversion and recombinase dimerization. However, some parameter combinations result in a predominance of these rapid fluctuations in the recombinase level, due to very rapid cycles of promoter inversion. This fast switching occurs in particular when the switching rate and the dilution/degradation rates are large. In these particular cases of predominant fast switching, the distribution of inter-peak times of the autocorrelation function shows a small variance, so the slope of the coherence plot remains low, even though the peak levels of recombinase may be irregular. This points to the fact that our coherence analysis cannot discriminate between a dominant fast switching regime and slower, coherent oscillations. This is how the NF with its fast switching appears so successful by this metric. Another challenge in our approach is posed by the duration of the stochastic simulation. When examining stochastic signals, the peaks of the autocorrelation function depend significantly on the window of observation of the signal: the autocorrelation peaks obtained from a short observation window should differ from those computed from a long observation window, which are likely to be smaller and present more variability due to noise. In addition, computing the autocorrelation function of an ensemble of extended stochastic trajectories is computationally demanding. Driven by these observations, we used a 40 h simulation window, but we verified that 5-fold longer simulations are qualitatively similar and indicate that oscillations are sustained for all the circuits we examined (Figure S1).

Summary of simulation results

Overall, the key finding of our computational analysis is that all the architectures we proposed have the capacity to exhibit coherent oscillations in a range of parameters. This finding indicates that diverse experimental implementations of recombinase oscillators are likely to succeed. Table 1 summarizes the most salient features and behavior of the different designs. We defined an incoherence metric to assess the effect of individual parameters on the ability of the circuits to produce oscillations. We found that the protein dilution/degradation rate constant parameter δ has a strong influence on the viability of our candidate oscillators; in particular, in all designs, a small δ (slow degradation) is detrimental to achieving coherent oscillations, while a large δ (fast degradation) may have either beneficial or detrimental effects depending on the circuit architecture. The R and NF designs have the smallest number of components and achieve coherent oscillations, with the NF design achieving the smallest incoherence; the R design is particularly sensitive to δ and the coherence of oscillations degrades as this parameter increases. For both circuits, coherence improves with larger values of translation parameter ρ. The RR and RP designs show incoherence trends comparable with the R circuit, except a large value of δ decreases their incoherence. The RR and RA designs also allow for the simple integration of a coupled process via another gene that is either repressed or activated, respectively. Implementing a coupled process by creating a system that alternates between producing one and two RNAs in the other designs would be more difficult to implement because it would require the integration of an operon at the inverting promoter. All designs are essentially unaffected by changes in the association rate parameter of the dimers, a_1, unless the value is decreased by a factor of 100 or more. Overall, the RR, RP, RS, and NF designs, which are the ones with an inhibitory element explicitly present in their cascade with the exception of the NF design, have comparable performance in terms of incoherence.

DISCUSSION

We described and computationally modeled different molecular circuit architectures to induce periodic behaviors using recombinases and we found that coherent oscillators are achievable by all the

Table 1. Summary of the features of the architectures we considered. Incoherence metric is abbreviated as IM

Circuit	Number of genes	Max Incoherence	Sensitivity to degradation δ	Sensitivity to rec. translation ρ, ρ_1	Sensitivity to TX/TL of regulators θ, ρ_2
R Design (Figure 3A)	2	13	IM increases with δ	IM decreases with ρ	N/A
RR Design (Figure 3B)	4	11	IM decreases with δ	IM decreases with ρ_1	IM increases with ρ_2
RP Design (Figure 3C)	4	9.5	IM insensitive with δ	IM decreases with ρ_1	IM increases with ρ_2
RA Design (Figure 4A)	4	12	IM increases with δ	IM decreases with ρ_1	IM insensitive with ρ_2
RS Design (Figure 4B)	4	15	IM increases with δ	IM decreases with ρ_1	IM insensitive with θ
NF Design (Figure 4C)	2	8.5	IM increases with δ	IM decreases with ρ	N/A

architectures we considered. At the core of all our designs, two self-inhibiting loops are coupled through a target DNA site that undergoes periodic inversion (switching) cycles induced by recombinase expression. We examined six variants of this basic architecture that use various mechanisms to introduce tighter control of recombinase levels in the circuit with the goal of achieving regular oscillations. Each of these oscillators was examined using stochastic simulations assuming that a single copy of each genetic component is present, capturing a realistic scenario for genomically integrated circuits. To evaluate the incoherence of oscillations, we used an approach that examines the statistics of the autocorrelation function of stochastic trajectories, and we used this metric to identify which kinetic rate constants improve oscillation coherence. Our simulations indicate that combining recombinases and mechanisms to suppress or delay recombinase expression, such as sequestration, transcriptional repressors, and proteases, allows to maintain or improve coherence. The positive effect of sequestration on the coherence of oscillations of the well-known repressilator circuit was previously observed experimentally and computationally through analysis of incoherence similar to ours.[11]

Our circuit designs are unique in that they couple two stable negative feedback loops through mutual activation, enabled by recombinase-mediated inversion of a target DNA site. This strategy departs from the traditional approach of designing molecular oscillators by including an overall negative feedback loop that can be destabilized via high gain, delays, or positive feedback.[4–9] Our computational simulations indicate that the parameters related to each individual self-inhibiting module influence the coherence of oscillations for the full circuit by determining the statistics of the peak amplitude and duration of each half-cycle (Figure 6). We speculate that, in experiments, these recombinase-based self-inhibiting modules may first be tuned individually, facilitating the synthesis and characterization of the complete oscillators. We also conjecture that nested clocks with multiple synchronized periods may be built by coupling different self-inhibiting components. Our computations suggest that periodic behaviors are likely to occur in a broad range of parameter values, supporting experimental realization of recombinase oscillators.

STAR★METHODS

Detailed methods are provided in the online version of this paper and include the following:

- KEY RESOURCES TABLE
- RESOURCE AVAILABILITY
  - Lead contact
  - Data and code availability
- EXPERIMENTAL MODELS AND SUBJECT DETAILS
- METHOD DETAILS
  - Reactions modeling an individual self-inhibiting module
  - Activator-recombinase oscillator: AR design
  - Recombinase and small-RNA: RS design
  - Negative feedback: NF design
- QUANTIFICATION AND STATISTICAL ANALYSIS
- ADDITIONAL RESOURCES

SUPPLEMENTAL INFORMATION

Supplemental information can be found online at https://doi.org/10.1016/j.isci.2022.105624.

ACKNOWLEDGMENTS

E.F. and C.C.S. acknowledge support by BBRSC-NSF/BIO award 2020039 and by NSF CCF/SHF award 2107483. J.L. acknowledges support by the B.I.G. program at UCLA. G.G. acknowledges support by the Strategic Grant MOSES at the University of Trento.

AUTHOR CONTRIBUTIONS

Conceptualization: C.C.S. and E.F.; Methodology and Investigation: C.C.S., G.G., and E.F.; Formal Analysis: J.L. and C.C.S.; Visualization: J.L. and C.C.S.; Data Curation: J.L. and C.C.S.; Writing - Original Draft, J.L., C.C.S., G.G., and E.F.; Writing - Review & Editing: J.L., C.C.S., G.G., and E.F. Project Administration: E.F.; Funding Acquisition: E.F.

Received: November 2, 2021
Revised: June 17, 2022
Accepted: November 15, 2022
Published: January 20, 2023

REFERENCES

1. Romond, P.C., Guilmot, J.M., and Goldbeter, A. (1994). The mitotic oscillator: temporal self-organization in a phosphorylation-dephosphorylation enzymatic cascade. Berichte der Bunsengesellschaft für. physikalische Chemie *98*, 1152–1159.

2. Barkai, N., and Leibler, S. (2000). Circadian clocks limited by noise. Nature *403*, 267–268.

3. Uriu, K., Morishita, Y., and Iwasa, Y. (2010). Synchronized oscillation of the segmentation clock gene in vertebrate development. J. Math. Biol. *61*, 207–229.

4. Novák, B., and Tyson, J.J. (2008). Design principles of biochemical oscillators. Nat. Rev. Mol. Cell Biol. *9*, 981–991.

5. Shitiri, E., Vasilakos, A., and Cho, H.-S. (2018). Biological oscillators in nanonetworks—opportunities and challenges. Sensors *18*, 1544.

6. Blanchini, F., Cuba Samaniego, C., Franco, E., and Giordano, G. (2018). Homogeneous time constants promote oscillations in negative feedback loops. ACS Synth. Biol. *7*, 1481–1487.

7. Bratsun, D., Volfson, D., Tsimring, L.S., and Hasty, J. (2005). Delay-induced stochastic oscillations in gene regulation. Proc. Natl. Acad. Sci. USA *102*, 14593–14598.

8. Cuba Samaniego, C., Giordano, G., Kim, J., Blanchini, F., and Franco, E. (2016). Molecular titration promotes oscillations and bistability in minimal network models with monomeric regulators. ACS Synth. Biol. *5*, 321–333.

9. Gonze, D., and Abou-Jaoudé, W. (2013). The goodwin model: behind the hill function. PLoS One *8*, e69573.

10. Purcell, O., Savery, N.J., Grierson, C.S., and Di Bernardo, M. (2010). A comparative analysis of synthetic genetic oscillators. J. R. Soc. Interface *7*, 1503–1524.

11. Potvin-Trottier, L., Lord, N.D., Vinnicombe, G., and Paulsson, J. (2016). Synchronous long-term oscillations in a synthetic gene circuit. Nature *538*, 514–517.

12. Riglar, D.T., Richmond, D.L., Potvin-Trottier, L., Verdegaal, A.A., Naydich, A.D., Bakshi, S., Leoncini, E., Lyon, L.G., Paulsson, J., and Silver, P.A. (2019). Bacterial variability in the mammalian gut captured by a single-cell synthetic oscillator. Nat. Commun. *10*, 4665.

13. Santos-Moreno, J., Tasiudi, E., Stelling, J., and Schaerli, Y. (2020). Multistable and dynamic CRISPRi-based synthetic circuits. Nat. Commun. *11*, 2746.

14. Merrick, C.A., Zhao, J., and Rosser, S.J. (2018). Serine integrases: advancing synthetic biology. ACS Synth. Biol. *7*, 299–310.

15. Guiziou, S., Mayonove, P., and Bonnet, J. (2019). Hierarchical composition of reliable recombinase logic devices. Nat. Commun. *10*, 456.

16. Kim, T., Weinberg, B., Wong, W., and Lu, T.K. (2021). Scalable recombinase-based gene expression cascades. Nat. Commun. *12*, 2711.

17. Pokhilko, A., Ebenhöh, O., Stark, W.M., and Colloms, S.D. (2018). Mathematical model of a serine integrase-controlled toggle switch with a single input. J. R. Soc. Interface *15*, 20180160.

18. Zhao, J., Pokhilko, A., Ebenhöh, O., Rosser, S.J., and Colloms, S.D. (2019). A single-input binary counting module based on serine integrase site-specific recombination. Nucleic Acids Res. *47*, 4896–4909.

19. Meinke, G., Bohm, A., Hauber, J., Pisabarro, M.T., and Buchholz, F. (2016). Cre recombinase and other tyrosine recombinases. Chem. Rev. *116*, 12785–12820.

20. Siuti, P., Yazbek, J., and Lu, T.K. (2013). Synthetic circuits integrating logic and memory in living cells. Nat. Biotechnol. *31*, 448–452.

21. Bonnet, J., Subsoontorn, P., and Endy, D. (2012). Rewritable digital data storage in live cells via engineered control of recombination directionality. Proc. Natl. Acad. Sci. USA *109*, 8884–8889.

22. Fernandez-Rodriguez, J., Yang, L., Gorochowski, T.E., Gordon, D.B., and Voigt, C.A. (2015). Memory and combinatorial logic based on dna inversions: dynamics and evolutionary stability. ACS Synth. Biol. *4*, 1361–1372.

23. Folliard, T., Steel, H., Prescott, T.P., Wadhams, G., Rothschild, L.J., and Papachristodoulou, A. (2017). A synthetic recombinase-based feedback loop results in robust expression. ACS Synth. Biol. *6*, 1663–1671.

24. Steel, H., and Papachristodoulou, A. (2019). Low-burden biological feedback controllers for near-perfect adaptation. ACS Synth. Biol. *8*, 2212–2219.

25. Samaniego, C.C., Giordano, G., and Franco, E. (2019). Periodic switching in a recombinase-based molecular circuit. IEEE Control Syst. Lett. *4*, 241–246.

26. Weinberg, B.H., Pham, N.T.H., Caraballo, L.D., Lozanoski, T., Engel, A., Bhatia, S., and Wong, W.W. (2017). Large-scale design of robust genetic circuits with multiple inputs and outputs for mammalian cells. Nat. Biotechnol. *35*, 453–462.

27. Weinberg, B.H., Cho, J.H., Agarwal, Y., Pham, N.T.H., Caraballo, L.D., Walkosz, M., Ortega, C., Trexler, M., Tague, N., Law, B., et al.

(2019). High-performance chemical-and light-inducible recombinases in mammalian cells and mice. Nat. Commun. *10*, 4845.

28. Gillespie, D.T. (1977). Exact stochastic simulation of coupled chemical reactions. J. Phys. Chem. *81*, 2340–2361.

29. Kuo, J., Yuan, R., Sánchez, C., Paulsson, J., and Silver, P.A. (2020). Toward a translationally independent rna-based synthetic oscillator using deactivated crispr-cas. Nucleic Acids Res. *48*, 8165–8177.

30. Yan, J. (2020). Identifying Hard Bounds on Molecular Fluctuation in Stochastic Reaction Systems (Harvard University). PhD thesis.

31. Olorunniji, F.J., McPherson, A.L., Rosser, S.J., Smith, M.C.M., Colloms, S.D., and Stark, W.M. (2017). Control of serine integrase recombination directionality by fusion with the directionality factor. Nucleic Acids Res. *45*, 8635–8645.

32. Buchler, N.E., and Louis, M. (2008). Molecular titration and ultrasensitivity in regulatory networks. J. Mol. Biol. *384*, 1106–1119.

33. Glass, D.S., Jin, X., and Riedel-Kruse, I.H. (2021). Nonlinear delay differential equations and their application to modeling biological network motifs. Nat. Commun. *12*, 1788.

34. Prindle, A., Selimkhanov, J., Li, H., Razinkov, I., Tsimring, L.S., and Hasty, J. (2014). Rapid and tunable post-translational coupling of genetic circuits. Nature *508*, 387–391.

35. Fink, T., Lonzarić, J., Praznik, A., Plaper, T., Merljak, E., Leben, K., Jerala, N., Lebar, T., Strmšek, Ž., Lapenta, F., et al. (2019). Design of fast proteolysis-based signaling and logic circuits in mammalian cells. Nat. Chem. Biol. *15*, 115–122.

36. Gao, X.J., Chong, L.S., Kim, M.S., and Elowitz, M.B. (2018). Programmable protein circuits in living cells. Science *361*, 1252–1258.

37. Kim, J.K., and Sontag, E.D. (2017). Reduction of multiscale stochastic biochemical reaction networks using exact moment derivation. PLoS Comput. Biol. *13*, e1005571.

38. Fern, J., Scalise, D., Cangialosi, A., Howie, D., Potters, L., and Schulman, R. (2017). Dna strand-displacement timer circuits. ACS Synth. Biol. *6*, 190–193.

STAR★METHODS

KEY RESOURCES TABLE

REAGENT or RESOURCE	SOURCE	IDENTIFIER
Software and algorithms		
Python Computer Software	Python Core Development Team	https://python.org
NumPy	NumPy Development Team	https://numpy.org
SciPy	SciPy Development Team	https://scipy.org
GitHub	Github Development Team	https://github.com

RESOURCE AVAILABILITY

Lead contact

Further information should be directed to Elisa Franco (Email:efranco@seas.ucla.edu).

Data and code availability

Stochastic simulations were implemented using custom scripts in Python and biocircuits package using a workstation with the following specifications: 8 GB RAM and a 2.9 GHz, dual-core Intel Core i5. Scripts are available on GitHub https://github.com/ccubasam-code/Recombinase-Oscillators.

EXPERIMENTAL MODELS AND SUBJECT DETAILS

None.

METHOD DETAILS

Reactions modeling an individual self-inhibiting module

$$\begin{aligned}
&\text{Transcription:} && S_R^{00} \xrightarrow{\theta} S_R^{00} + M \\
&\text{mRNA Degradation:} && M \xrightarrow{\varphi} \varnothing \\
&\text{Translation:} && M \xrightarrow{\rho} M + Z \\
&\text{Homodimerization:} && Z + Z \underset{d_1}{\overset{a_1}{\rightleftharpoons}} X \\
&\text{Protein Degradation:} && Z, X \xrightarrow{\delta} \varnothing \\
&\text{Binding/Unbinding:} && X + S_R^{00} \underset{d_0}{\overset{a_0}{\rightleftharpoons}} S_R^{10} \qquad X + S_R^{10} \underset{d_0}{\overset{a_0}{\rightleftharpoons}} S_R^{11} \\
& && X + S_R^{00} \underset{d_0}{\overset{a_0}{\rightleftharpoons}} S_R^{01} \qquad X + S_R^{01} \underset{d_0}{\overset{a_0}{\rightleftharpoons}} S_R^{11} \\
&\text{Inversion:} && S_R^{11} \xrightarrow{r} S_L^{00} + 2X.
\end{aligned}$$

Activator-recombinase oscillator: AR design

An inverting promoter regulates the transcription of either of the two mRNA activators, W_1 and W_2, with rate β at any given time. W_1 is produced when the promoter is pointing to the right (configuration S_R), and W_2 is produced when the promoter is pointing to the left (configuration S_L). The mRNAs also decay with a rate constant φ.

$$\begin{aligned}
&\text{Transcription:} && S_R^{00} \xrightarrow{\beta} S_R^{00} + W_1 \qquad S_L^{00} \xrightarrow{\beta} S_L^{00} + W_2 \\
&\text{mRNA Degradation:} && W_1 \xrightarrow{\varphi} \varnothing \qquad W_2 \xrightarrow{\varphi} \varnothing.
\end{aligned}$$

W_1 and W_2 are translated into activators proteins Y_1 and Y_2 with a rate constant ρ_2, and decay with a rate constant δ.

$$\begin{array}{ll} \text{Translation:} & W_1 \xrightarrow{\rho_2} W_1 + Y_1 \qquad W_2 \xrightarrow{\rho_2} W_2 + Y_2 \\ \text{Protein Degradation:} & Y_1 \xrightarrow{\delta} \varnothing \qquad Y_2 \xrightarrow{\delta} \varnothing. \end{array}$$

The activators Y_1 and Y_2 bind and unbind to target promoters P_1 and P_2 with association rate constant a_R and dissociation rate constant d_R, respectively. The bound promoters P_1^*, and P_2^* regulate the transcription of recombinase mRNAs M_1 and M_2 with rate θ. Both mRNAs decay with a rate constant φ. In addition, the mRNAs produce recombinase monomers Z_1 and Z_2 with a rate constant ρ_1.

$$\begin{array}{ll} \text{Binding/Unbinding:} & Y_1 + P_1 \underset{d_R}{\overset{a_R}{\rightleftharpoons}} P_1^* \qquad Y_2 + P_2 \underset{d_R}{\overset{a_R}{\rightleftharpoons}} P_2^* \\ \text{Transcription:} & P_1^* \xrightarrow{\theta} P_1^* + M_1 \qquad P_2^* \xrightarrow{\theta} P_2^* + M_2 \\ \text{mRNA Degradation:} & M_1 \xrightarrow{\varphi} \varnothing \qquad M_2 \xrightarrow{\varphi} \varnothing \\ \text{Translation:} & M_1 \xrightarrow{\rho_1} M_1 + Z_1 \qquad M_2 \xrightarrow{\rho_1} M_2 + Z_2. \end{array}$$

The monomers Z_1 and Z_2 form homodimers X_1 and X_2 in addition to heterodimer C, both with an association rate constant a_1 and a dissociation rate constant d_1. The heterodimer formation is possible because the second recombinase monomer is fused to its RDF. In addition, all proteins complexes decay with a rate constant δ.

$$\begin{array}{ll} \text{Homodimerization:} & Z_1 + Z_1 \underset{d_1}{\overset{a_1}{\rightleftharpoons}} X_1 \qquad Z_2 + Z_2 \underset{d_1}{\overset{a_1}{\rightleftharpoons}} X_2 \\ \text{Heterodimerization:} & Z_1 + Z_2 \underset{d_1}{\overset{a_1}{\rightleftharpoons}} C. \\ \text{Protein Degradation:} & Z_1, X_1, Z_2, X_2, C \xrightarrow{\delta} \varnothing \end{array}$$

Finally, the switching rate of the promoter is regulated by the recombinase dimers X_1 and X_2 which bind to the promoter with an association rate constant of a_0 and a dissociation rate constant of d_0.

$$\begin{array}{ll} \text{Binding/Unbinding:} & X_1 + S_L^{00} \underset{d_0}{\overset{a_0}{\rightleftharpoons}} S_L^{10} \qquad X_1 + S_L^{10} \underset{d_0}{\overset{a_0}{\rightleftharpoons}} S_L^{11} \\ & X_1 + S_L^{00} \underset{d_0}{\overset{a_0}{\rightleftharpoons}} S_L^{01} \qquad X_1 + S_L^{01} \underset{d_0}{\overset{a_0}{\rightleftharpoons}} S_L^{11} \\ \text{Binding/Unbinding:} & X_2 + S_R^{00} \underset{d_0}{\overset{a_0}{\rightleftharpoons}} S_R^{10} \qquad X_2 + S_R^{10} \underset{d_0}{\overset{a_0}{\rightleftharpoons}} S_R^{11} \\ & X_2 + S_R^{00} \underset{d_0}{\overset{a_0}{\rightleftharpoons}} S_R^{01} \qquad X_2 + S_R^{01} \underset{d_0}{\overset{a_0}{\rightleftharpoons}} S_R^{11} \\ \text{Inversion:} & S_L^{11} \xrightarrow{r} S_R^{00} \qquad S_R^{11} \xrightarrow{r} S_L^{00} \end{array}$$

Recombinase and small-RNA: RS design

The promoter regulates the transcription of either of the two small RNAs, W_1 and W_2, with rate β at any given time. The mRNAs also decay with a rate constant φ.

$$\begin{array}{ll} \text{Transcription:} & \varnothing \xrightarrow{\beta} W_1 \qquad \varnothing \xrightarrow{\beta} W_2 \\ \text{mRNA Degradation:} & W_1 \xrightarrow{\varphi} \varnothing \qquad W_2 \xrightarrow{\varphi} \varnothing. \end{array}$$

W_1 and W_2 sequester the mRNA M_1 and M_2, respectively, at a rate constant ψ.

$$\text{mRNASequestration} : \mathrm{W_1} + \mathrm{M_1} \xrightarrow{\psi} \varnothing \, \mathrm{W_2} + \mathrm{M_2} \xrightarrow{\psi} \varnothing.$$

The promoter pointing to the left and right up-regulates the transcription of recombinase mRNAs M_1, and M_2 with rate θ. Both mRNAs decay with a rate constant φ. In addition, the mRNAs produce recombinase monomers Z_1 and Z_2 with a rate constant ρ_1.

$$\begin{array}{ll} \text{Transcription:} & S_L^{00} \xrightarrow{\theta} S_L^{00} + M_1 \qquad S_R^{00} \xrightarrow{\theta} S_R^{00} + M_2 \\ \text{mRNA Degradation:} & M_1 \xrightarrow{\varphi} \varnothing \qquad M_2 \xrightarrow{\varphi} \varnothing \\ \text{Translation:} & M_1 \xrightarrow{\rho_1} M_1 + Z_1 \qquad M_2 \xrightarrow{\rho_1} M_2 + Z_2. \end{array}$$

The monomers Z_1 and Z_2 form homodimers X_1 and X_2 in addition to heterodimer C, both with an association rate constant a_1 and a dissociation rate constant d_1. The heterodimer formation is possible because the second recombinase monomer is fused to its RDF. In addition, all proteins complexes decay with a rate constant δ.

Homodimerization:	$Z_1 + Z_1 \underset{d_1}{\overset{a_1}{\rightleftharpoons}} X_1$	$Z_2 + Z_2 \underset{d_1}{\overset{a_1}{\rightleftharpoons}} X_2$
Heterodimerization:	$Z_1 + Z_2 \underset{d_1}{\overset{a_1}{\rightleftharpoons}} C.$	
Protein Degradation:	$Z_1, X_1, Z_2, X_2, C \xrightarrow{\delta} \varnothing$	

Finally, the switching rate of the promoter is regulated by the recombinase dimers X_1 and X_2 which bind and unbind to the promoter with rate constants a_0 and d_0, respectively.

Binding/Unbinding:	$X_1 + S_L^{00} \underset{d_0}{\overset{a_0}{\rightleftharpoons}} S_L^{10}$	$X_1 + S_L^{10} \underset{d_0}{\overset{a_0}{\rightleftharpoons}} S_L^{11}$
	$X_1 + S_L^{00} \underset{d_0}{\overset{a_0}{\rightleftharpoons}} S_L^{01}$	$X_1 + S_L^{01} \underset{d_0}{\overset{a_0}{\rightleftharpoons}} S_L^{11}$
Binding/Unbinding:	$X_2 + S_R^{00} \underset{d_0}{\overset{a_0}{\rightleftharpoons}} S_R^{10}$	$X_2 + S_R^{10} \underset{d_0}{\overset{a_0}{\rightleftharpoons}} S_R^{11}$
	$X_2 + S_R^{00} \underset{d_0}{\overset{a_0}{\rightleftharpoons}} S_R^{01}$	$X_2 + S_R^{01} \underset{d_0}{\overset{a_0}{\rightleftharpoons}} S_R^{11}$
Inversion:	$S_L^{11} \xrightarrow{r} S_R^{00}$	$S_R^{11} \xrightarrow{r} S_L^{00}$

Negative feedback: NF design

mRNA M_1 is produced constitutively at a rate of θ_1 while the mRNA M_2 is only produced when the promoter points to the right at a rate of θ_2. Both mRNAs are assumed to dilute/degrade with a rate constant φ. In addition, the mRNAs M_1 and M_2 are translated to recombinase monomers Z_1 and Z_2, respectively, with rate constant ρ.

Transcription:	$\varnothing \xrightarrow{\theta_1} M_1$	$S_R^{00} \xrightarrow{\theta_2} S_R^{00} + M_2$
mRNA Degradation:	$M_1 \xrightarrow{\varphi} \varnothing$	$M_2 \xrightarrow{\varphi} \varnothing$
Translation:	$M_1 \xrightarrow{\rho} M_1 + Z_1$	$M_2 \xrightarrow{\rho} M_2 + Z_2$

The serine recombinase monomers Z_1 and Z_2 can form the homodimers X_1 and X_2, respectively. Since Z_2 is Z_1 fused to its RDF, the two species can also form the heterodimer C. For simplicity, we assume all dimers have an association rate constant a_1 and a dissociation rate constant d_1. In addition, we assume all proteins degrade with a rate constant δ.

Homodimerization:	$Z_1 + Z_1 \underset{d_1}{\overset{a_1}{\rightleftharpoons}} X_1$	$Z_2 + Z_2 \underset{d_1}{\overset{a_1}{\rightleftharpoons}} X_2$
Heterodimerization:	$Z_1 + Z_2 \underset{d_1}{\overset{a_1}{\rightleftharpoons}} C.$	
Protein Degradation:	$Z_1, X_1, Z_2, X_2, C \xrightarrow{\delta} \varnothing$	

The rate of promoter inversion is regulated by the recombinase dimers X_1 and X_2 with binding and unbinding rates a_0 and d_0, respectively, and the inversion rate r.

Binding/Unbinding:	$X_1 + S_L^{00} \underset{d_0}{\overset{a_0}{\rightleftharpoons}} S_L^{10}$	$X_1 + S_L^{10} \underset{d_0}{\overset{a_0}{\rightleftharpoons}} S_L^{11}$
	$X_1 + S_L^{00} \underset{d_0}{\overset{a_0}{\rightleftharpoons}} S_L^{01}$	$X_1 + S_L^{01} \underset{d_0}{\overset{a_0}{\rightleftharpoons}} S_L^{11}$
Binding/Unbinding:	$X_2 + S_R^{00} \underset{d_0}{\overset{a_0}{\rightleftharpoons}} S_R^{10}$	$X_2 + S_R^{10} \underset{d_0}{\overset{a_0}{\rightleftharpoons}} S_R^{11}$
	$X_2 + S_R^{00} \underset{d_0}{\overset{a_0}{\rightleftharpoons}} S_R^{01}$	$X_2 + S_R^{01} \underset{d_0}{\overset{a_0}{\rightleftharpoons}} S_R^{11}$
Inversion:	$S_L^{11} \xrightarrow{r} S_R^{00}$	$S_R^{11} \xrightarrow{r} S_L^{00}$

QUANTIFICATION AND STATISTICAL ANALYSIS

Statistical analyses were performed using the mean over 500 trajectories from the stochastic simulations.

ADDITIONAL RESOURCES

None.